Surface, Structural, Optical, and Thermal Stability Analysis in PM6 and D18-Cl Based Non-Fullerene Acceptor Organic Thin Film Blends

Hissah Mutlaq Alqabbani, Alanoud Abdullah Alfozan, Prof. Dr. Emiliano Cortés, Prof. Dr. Frédéric Laquai

hissah.alqabbani@kaust.edu.sa, alanoud.alfozan@kaust.edu.sa, Emiliano.Cortes@lmu.de, frederic.laquai@lmu.de

Abstract

Organic solar cells offer distinct advantages in flexibility, lightweight design, and semi-transparency, yet poor long-term operational stability remains a barrier to commercial deployment. This project studies the structural and chemical stability of organic solar cells. State-of-the-art organic blend thin films are fabricated via spin-coating from chloroform as a solvent using polymer donors (PM6, D18-Cl) paired with non-fullerene acceptors (Y6, Y12) in an inert nitrogen environment. The project uses ultraviolet (UV), visible (Vis), and near-infrared (NIR) absorption spectroscopy to evaluate optical properties, confirming strong optical complementarity across all donor:acceptor blends. Furthermore, this project evaluates the thermal degradation of selected blend films by applying progressive thermal stress up to 300 °C, with each 10 minute heating step performed on a hot plate in a nitrogen environment. The absorption spectral analysis revealed optimal absorption at 140°C for D18-Cl:Y6, and 180 °C for PM6:Y6; heating to 300 °C induced a significant breakdown in both blends. X-ray Photoelectron Spectroscopy (XPS) and Raman spectroscopy were used to evaluate surface chemistry and molecular conformation. XPS confirmed the high chemical purity and stoichiometric integrity of the active layers. Raman analysis revealed that PM6 blends maintained conformational rigidity, whereas D18-Cl blends exhibited beneficial amorphous intermixing. Crucially, substituting the Y6 acceptor with Y12 preserved the donors' primary backbone vibrations and intrinsic hole-transport networks. These findings demonstrate that targeted alkyl chain engineering mitigates morphological degradation, enhancing the operational stability and commercial viability of organic photovoltaics.

Date: August 24, 2026

Contents

1 Introduction **2**

2 Related Work **4**

3 Methodology **4**

3.1 Synthesis . . . 4

3.2 UV-Vis Optical Absorption Spectroscopy . . . 5

3.3 X-ray Photoelectron Spectroscopy (XPS) . . . 6

3.4 Raman Spectroscopy . . . 7

4 Results **8**

4.1 Optical Characterization . . . 8

4.2 Thermal Stability and Degradation Analysis . . . 9

4.3 Surface Analysis . . . 10

4.4 Structural Profiling . . . 12

5 Discussion **13**

5.1 Optical Characterization . . . 13

5.2 Thermal Stability and Degradation Analysis . . . 13

5.3 XPS . . . 13

5.4 Raman Spectroscopy . . . 13

6 Limitations and Future Work **14**

7 Acknowledgment **14**

8 Conclusion **15**

References **15**

1 Introduction

Solar cell technology, a significant sector for renewable energy, relies heavily on inorganic semiconductors, even though they are energy-intensive, brittle, heavy and opaque [1]. To address these limitations, organic solar cells (OSCs) compete as an alternative, designed to overcome such challenges by being easy to manufacture, flexible, lightweight, and semi-transparent.

OSCs differ from inorganic cells in their active layer composition, which consists of a blend of organic semiconductors acting as both electron donors and acceptors. Typically, the donors are semiconducting polymers and the acceptors are small molecules. When sunlight is absorbed by the donor, an electron is excited from the HOMO to LUMO energy level, leaving a positively charged hole. This bound electron-hole pair is called an exciton. To conduct a charge, the exciton must be separated into free carriers at the donor-acceptor interface. For this separation to occur, the donor must have a higher LUMO level than the acceptor, providing the energetic driving force for the electron to transfer, as shown in Figure 1. Meanwhile, the donor's higher HOMO level ensures the hole remains in the donor phase, allowing both free charges to travel to their respective electrodes and generate electricity [2].

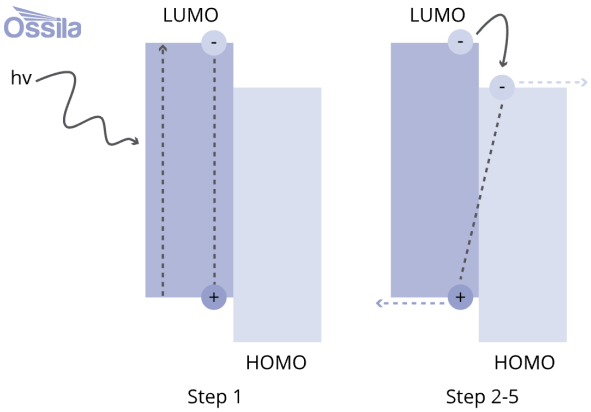


Figure 1 Energy level diagram illustrating photoexcitation and charge separation at the donor-acceptor interface [2].

To maximize charge separation, modern devices use a bulk hetero-junction (BHJ) architecture, which is a thin film consisting of a blended network of donor and acceptor materials. In contrast, a single-layered OSC consists purely of either a donor or an acceptor. Figure 2 emphasizes the difference in their structure.

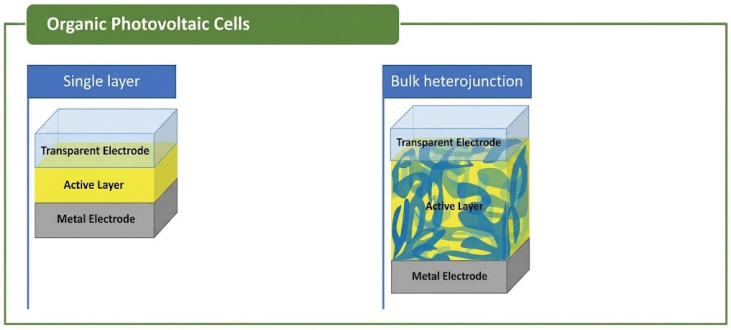
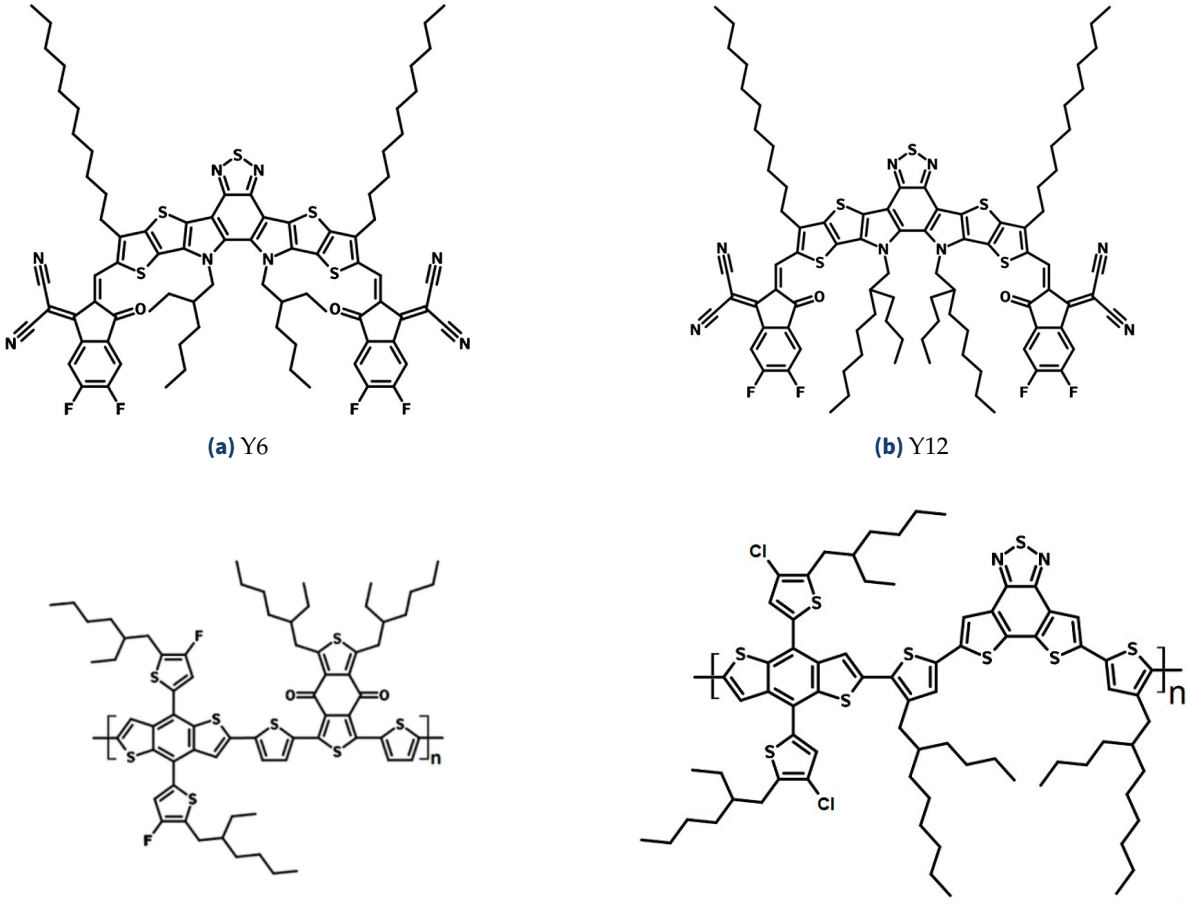


Figure 2 The device structure of a single-layer and a bulk heterojunction (BHJ) organic photovoltaic cell.

In this research, we initially synthesized four single-layered OSC thin-films to establish a baseline analysis, consisting of two non-fullerene small-molecule acceptors: Y6 and Y12, and two semiconducting polymer donors: PM6 and D18-Cl, whose chemical structures are illustrated in Figure 3. We then developed our primary BHJ thin-films by mixing these materials into four distinct blends: PM6:Y6, PM6:Y12, D18-Cl:Y6, and D18-Cl:Y12. The objective of this work is to characterize and analyze OSC single-layered and BHJ thin films by utilizing UV-Vis spectroscopy to investigate the optical absorption profiles and Raman spectroscopy to probe the internal morphology of these donor:acceptor blends. Concurrently, because high-performance donors and acceptors share similar elemental compositions, characterizing these materials using X-ray Photoelectron Spectroscopy (XPS) presents a significant analytical challenge. Their XPS photoemission signals overlap heavily when blended in active layers. To resolve this ambiguity and enable accurate future analysis of complex blends, this study establishes a rigorous chemical and energetic baseline by systematically characterizing the core-level spectra of pure, unblended PM6, D18-Cl, Y6, and Y12 films. This foundational reference library provides the exact mathematical constraints required to deconvolute complex spectra and accurately evaluate intrinsic surface properties. Subsequently, Raman spectroscopy is introduced as a complementary technique to probe the internal morphology of the blended films and investigate the active layers beyond the surface.



(a) Y6 **(b)** Y12

(c) PM6 **(d)** D18-Cl

Figure 3 Chemical structures of the investigated materials: (a) Y6, (b) Y12, (c) PM6, and (d) D18-Cl.

2 Related Work

To establish a fundamental understanding of XPS for this study, the comprehensive guide by Stevie and Donley [3] was utilized as a primary reference. This work served as a practical manual for our spectral analysis, providing essential guidance on the physical principles of surface sensitivity and binding energy shifts.

Additionally, the study by Zhang et al. [4] served as a crucial reference for understanding the specific core-level behaviors of PM6 and Y6. This paper helped identifying the intrinsic spectral signatures of these materials in their pristine states, particularly the binding energies associated with the PM6 sulfur backbone and Y6 cyano groups. This work validated our approach of studying pure, unblended active layers, providing a practical framework for mapping the baseline chemical states of high-performance organic semiconductors before evaluating complex blends.

3 Methodology

3.1 Synthesis

This section details the experimental procedures used for substrate preparation, solution formulation and the fabrication of the organic thin films. The overall process flow is illustrated in Figure 4. A step-by-step cleaning process was performed on glass substrates, as outlined below and in Figure 4.

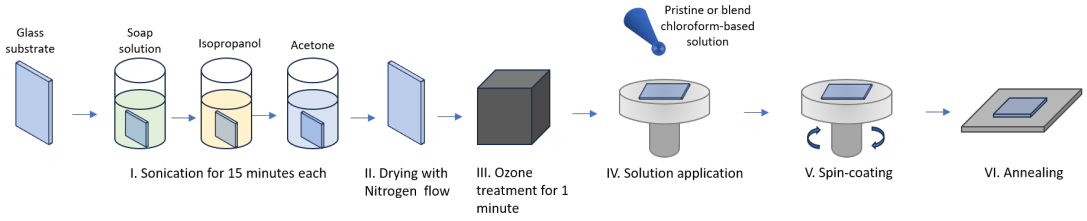


Figure 4 Schematic workflow of the thin film fabrication process.

- The substrates were initially rubbed with cotton swab and soap solution and were subsequently sonicated for 15 minutes each in the following solvents: soap solution, isopropanol, and acetone.
- After sonication, the substrates were thoroughly dried using a nitrogen flow.
- The substrates underwent an ozone treatment for 1 minute to remove any final trace and to improve wettability.

Both pristine material solutions and their blend counterparts were prepared using chloroform as the primary solvent. For the blend solutions of the PM6, a small amount of chloronaphthalene was added as a solvent additive.

Pristine solutions of D18-Cl, PM6, Y6, Y12 were formulated. The masses of the materials and the volume of the chloroform used are detailed in Table 1.

Four blend combinations were prepared in Chloroform with a fixed total material concentration of 16 mg/mL, namely PM6:Y6, PM6,Y12, D18-Cl:Y6,and D18-Cl:Y12. The mass ratios and formulations for the blends are provided in Table 2.

Table 1 Pristine solution formulation in Chloroform.

Material	Mass (mg)	Volume of Chloroform (mL)
Y6	6.67	0.76
Y12	4.34	0.5
PM6	6.12	0.84
D18-Cl	4.07	0.56

Table 2 Blend solution formulation in Chloroform.

Blend	Mass Ratio	Concentration(mg/mL)	Mass 1 (mg)	Mass 2 (mg)	Additive (vol%)
PM6:Y6	1:1.2	16	7.21	8.53	0.5 Chloronaphthalene
PM6:Y12	1:1.2	16	7.21	8.53	0.5 Chloronaphthalene
D18-Cl:Y6	1:1	16	8.26	8.30	0
D18-Cl:Y12	1:1	16	8.26	8.30	0

The prepared solutions were statically dispensed and spread across the pre-cleaned glass substrates to ensure full surface coverage. The subsequent stages involved spin coating and thermal annealing on a hot plate, following the general workflow shown in Figure 4.

The processing parameters, including spin-coating speed (rpm) and annealing conditions (temperature and time), for pristine materials and their blends are specified in Table 3. All pristine material films were processed without thermal annealing.

Table 3 Processing parameters for thin film fabrication.

Material	Spin-Coating Speed (rpm)	Annealing Temperature (°C)	Annealing Time (min)
All Pristine Materials	2000	N/A	N/A
PM6 Blends	2000	80	15
D18-Cl	4000	110	10

3.2 UV-Vis Optical Absorption Spectroscopy

The optical absorption spectra of both the pristine thin films and their respective blend films were acquired to investigate their light harvesting properties and absorption profiles across the ultraviolet, visible, and near-infrared regions. All absorption measurements were performed at room temperature using a PerkinElmer Lambda 1050 UV-Vis-NIR spectrometer, as schematically illustrated in Figure 5.

The acquisition settings used during testing were as follows:

- **Instrument:** PerkinElmer Lambda 1050 UV-Vis-NIR Spectrometer.
- **Measurement Mode:** Absorbance (Film on substrate).
- **Baseline Correction:** A clean, bare glass substrate was used as the reference baseline.

Prior to sample measurement, a baseline calibration was performed across the specified wavelength spectrum using a pre-clean glass substrate to subtract the substrate absorption effect. Pristine and blend thin films were sequentially mounted perpendicular to the incident light beam within the sample compartment. Optical absorption spectra were subsequently recorded to evaluate

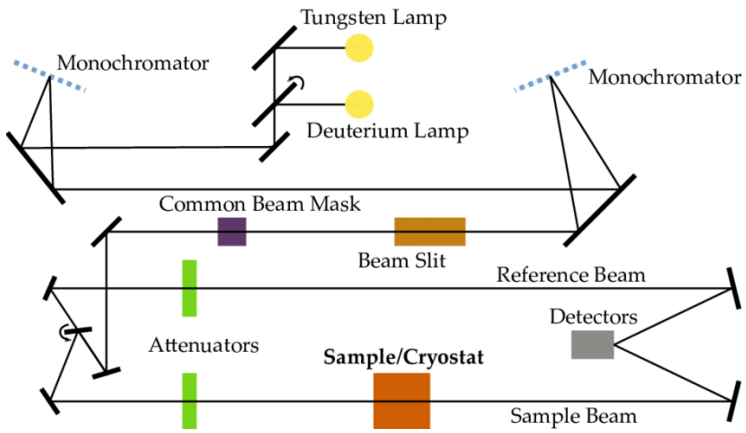


Figure 5 Schematic representation of the UV-Vis-NIR Spectrometer.

key parameters, including absorption edges, peak absorption wavelengths, and the influence of thermal annealing of high temperatures.

3.3 X-ray Photoelectron Spectroscopy (XPS)

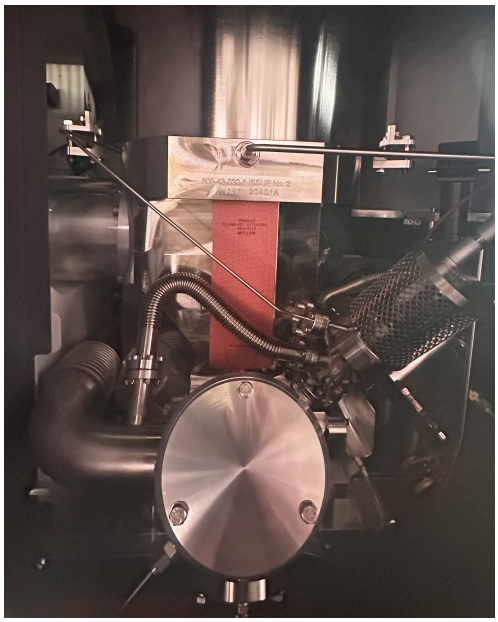
XPS is a sensitive surface analytical technique that probes the top 10 nm of a material to determine its elemental composition and chemical states. It operates on the photoelectric effect, where incident X-rays eject core-level electrons, providing critical insights into the chemical environment based on their binding energies. In details, by measuring the kinetic energy of these ejected electrons, their binding energy can be found using this equation:

$$BE = h\nu - KE - \Phi_{spec} \tag{1}$$

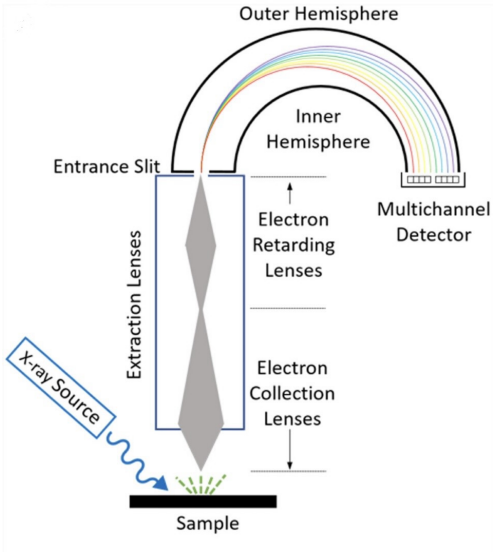
where BE is the binding energy, $h\nu$ is the X-ray photon energy, KE is the kinetic energy of the emitted electron, and Φ_{spec} is the spectrometer work function. A picture of the main chamber of XPS used in this research is shown in Figure 6a, where the entire system is maintained under an ultra-high vacuum (UHV) environment to ensure that emitted photoelectrons reach the detector without scattering off gas molecules and to prevent rapid surface contamination. Also, Figure 6b is provided for further clarification of the system. The XPS system consists of:

- **X-ray Source:** The X-ray gun irradiates the sample stage to excite the target materials.
- **Electron Extraction Lenses:** Positioned directly above the sample, these electrostatic lenses collect the emitted photoelectrons and retard their kinetic energy to a specific pass energy.
- **Hemispherical Analyzer and Detector:** The electrons are directed into the concentric hemispherical analyzer (shown at the top of Figure 6b). By applying specific voltages to the inner and outer hemispheres, only electrons with a matching energy can successfully traverse the curve to reach the multichannel detector [3].

For the spectral acquisition of the samples, the X-ray spot size was set to 200 μm. To neutralize potential surface charging during the measurements, an electron flood gun was actively utilized. The analytical sequence included an initial XPS survey and valence band scan, followed by targeted high-resolution core-level scans for S2p, C1s, N1s, O1s, and F1s. These high-resolution spectra were collected using a pass energy of 20.00 eV, a fine energy step size of 0.100 eV, and a dwell time of 50 ms. Each core-level region was accumulated over 5 scans to optimize the signal-to-noise ratio. Furthermore, to maintain precise focal distance, an auto-height optimization routine was executed across 41 points using a 50 μm step size.



(a) Picture of the main chamber of the XPS used for this experiment.

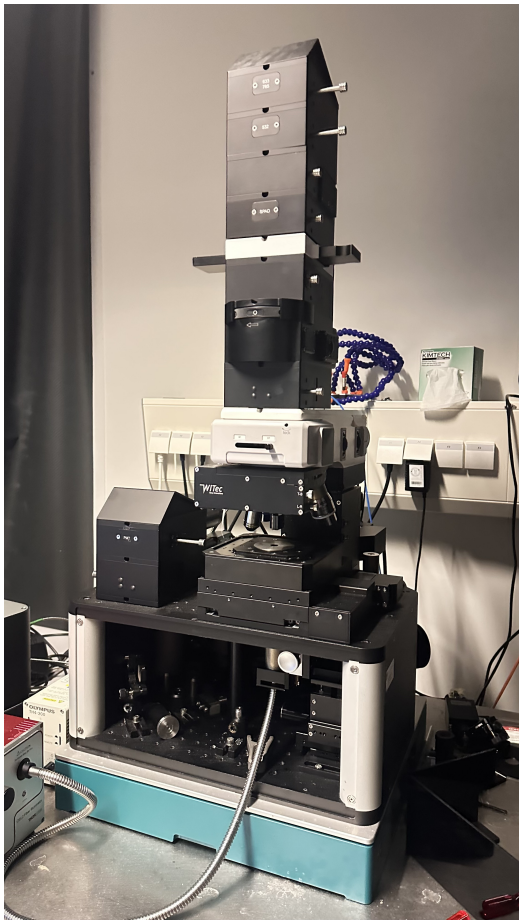


(b) XPS internal configuration [3].

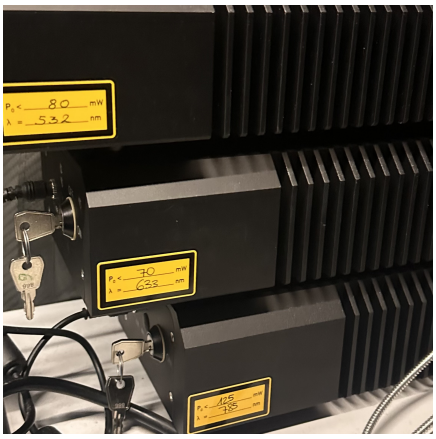
Figure 6 Overview of the XPS system.

3.4 Raman Spectroscopy

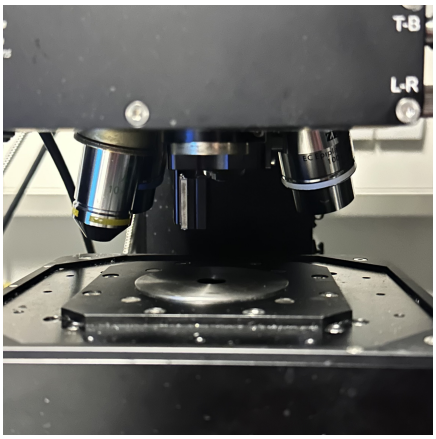
Raman spectroscopy is a structural molecular vibrations analysis technique based on the inelastic scattering of monochromatic light. By measuring the energy shift of scattered photons, it generates a structural fingerprint used to identify specific chemical bonds and evaluate molecular ordering. This method was implemented to evaluate the bulk molecular packing, phase distribution, and structural crystallinity of the active layers of the fully BHJ blends. The measurements were conducted using a high-resolution WITec confocal Raman microscope Figure 7a. To probe the vibrational modes of the organic semiconductors, the samples were excited using a multiline laser source Figure 7b. Specifically, a 632.72 nm laser was utilized and focused onto the sample through a 100x objective lens Figure 7c. The incident laser power was strictly maintained at 5.83 mW to prevent thermal degradation or photo-oxidation of the delicate thin films.



(a) The WITec confocal Raman microscope.



(b) The multiline laser source.



(c) The optical microscope objective turret.

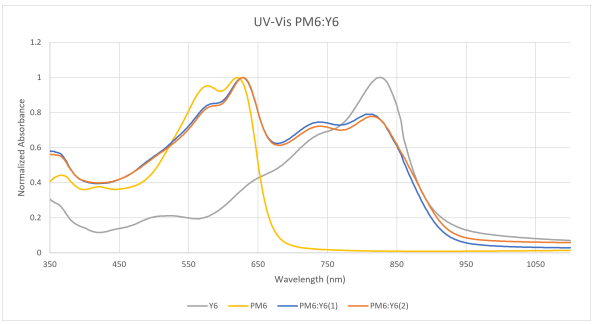
Figure 7 Key optical components of the Raman spectroscopy system.

4 Results

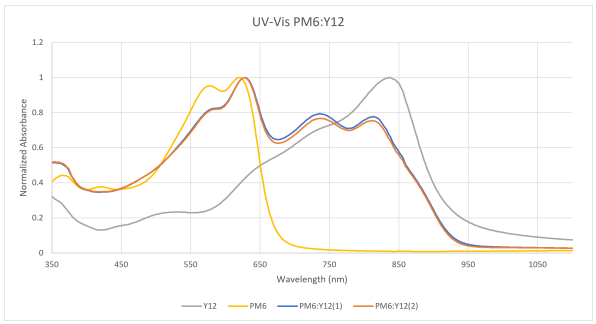
4.1 Optical Characterization

The optical absorption characteristics of pristine donor polymers, non-fullerene acceptors, and their corresponding BHJ thin films were investigated using absorption spectroscopy.

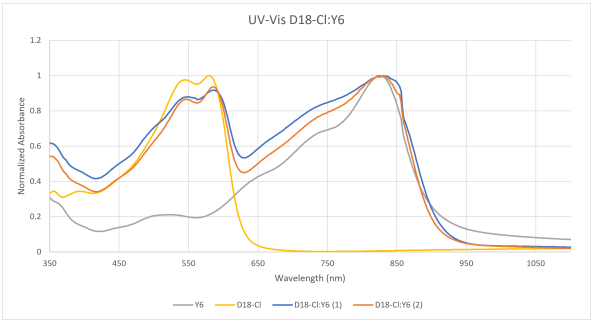
As shown in Figure 8a- 8d, all four blend combinations demonstrate strong optical complementarity across the visible and near-infrared regions. Pristine PM6 and D18-Cl exhibit primary absorption in the high energy 500-650 nm range. Conversely, Pristine Y6 and Y12 acceptors display strong absorption in the near-infrared between 650 nm and 850 nm, peaking near 825-840 nm. In each corresponding blend, the dual-band absorption profile successfully incorporates both donor and acceptor features.



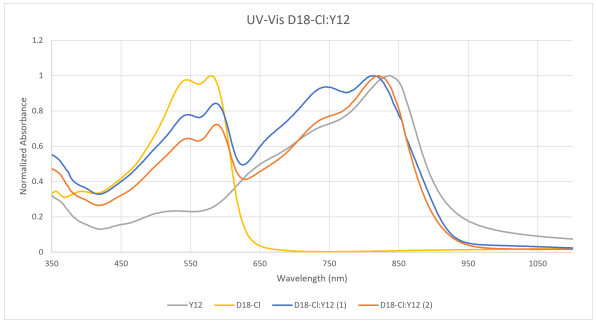
(a) PM6, Y6, and PM6:Y6 blend thin films.



(b) PM6, Y12, and PM6:Y12 blend thin films.



(c) D18-Cl, Y6, and D18-Cl:Y6 blend thin films.



(d) D18-Cl, Y12, and D18-Cl:Y12 blend thin films.

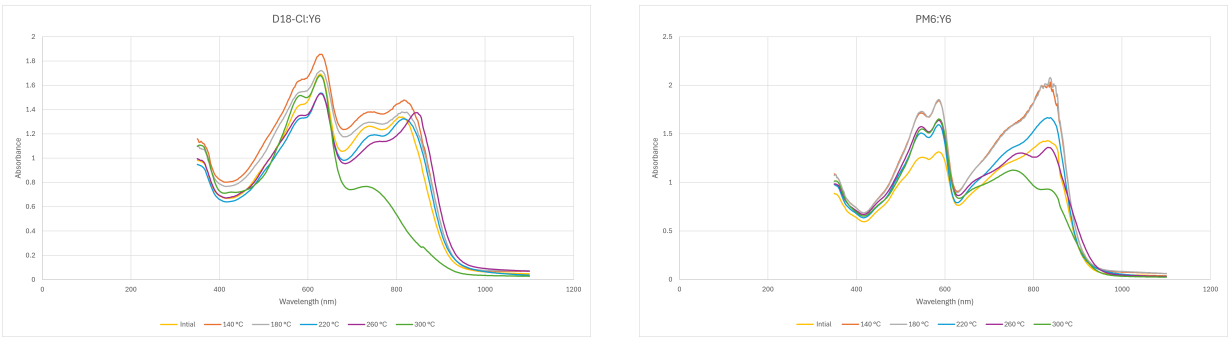
Figure 8 Normalized absorption spectra of all blend thin films.

4.2 Thermal Stability and Degradation Analysis

The thermal stability and degradation behavior of D18-Cl:Y6 and PM6:Y6 thin films were evaluated under progressive thermal stress up to 300°C , with each heating step performed on a hot plate for 10 minutes inside a nitrogen-filled glove-box.

For the D18-Cl:Y6 blend film shown in Figure 9a, heating from the initial baseline to 140 °C leads to an increase in overall absorbance, with strong donor peaks at 630 nm and acceptor peaks at 820 nm. Heating between 180 °C and 260 °C induces a decline in absorption accompanied by a slight red-shift of the acceptor absorption edge from approximately 815 nm to approximately 850 nm. At 300°C, the D18-Cl:Y6 film undergoes severe optical breakdown, marked by the sharp collapse of the near-infrared acceptor band down to an absorbance of 0.25.

The PM6:Y6 blend film exhibits distinct thermal degradation dynamics, as illustrated in Figure 9b. Thermal treatment up to 180 °C enhances overall film absorption. Increasing the temperature from 220°C to 260 °C results in a moderate drop in optical density while preserving the underlying peak positions. Upon reaching 300°C, the primary Y6 near-infrared absorption band collapses, whereas the PM6 donor peak retains significant absorbance.



(a) D18-Cl:Y6. **(b)** PM6:Y6.

Figure 9 Un-normalized absorption spectra under progressive thermal treatment.

4.3 Surface Analysis

XPS measurements of the pure donor (PM6, D18-Cl) and acceptor (Y6, Y12) films are presented. Figure 10 displays the sample holder loaded with the four pristine films inside the main XPS chamber. To ensure accurate chemical state determination, all binding energies were referenced to the adventitious carbon C1s peak at 284.8 eV to compensate for surface charging.

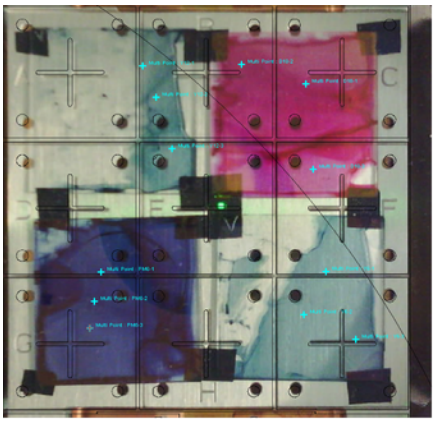


Figure 10 Platter view of the sample holder.

4.3.1 Atomic Ratios

The atomic ratios of the measurements are relatively close to the theoretical ratios according to Table 4.

4.3.2 High-resolution Spectra of Acceptors Y6 and Y12

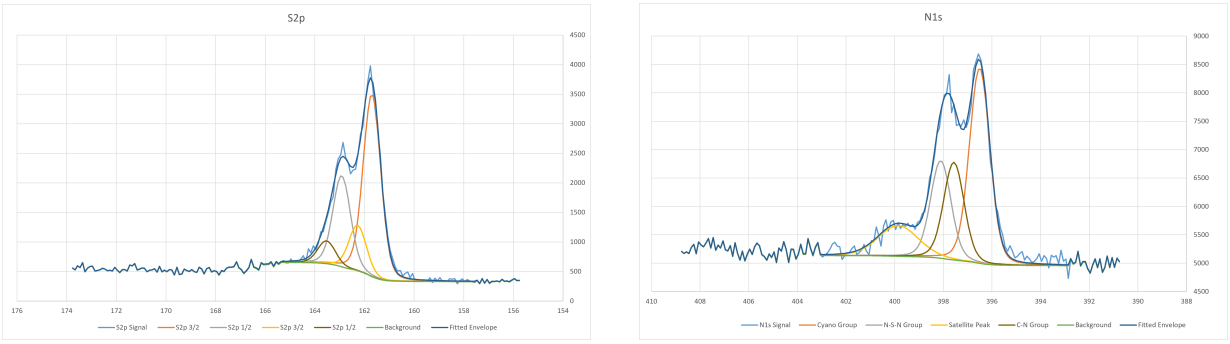
The core-level spectra for Y6 and Y12, as shown in Figure 11 and Figure 12, demonstrate $S2p_{3/2} - 2p_{1/2}$ spin-orbit splitting with a 1:2 doublet area ratio and $\Delta = 1.16$ eV, a 1:4 ratio between the thiophene C-S and N-S-N sulfur states, and a 2:2:4 ratio for the $C \equiv N$, C-N, and N-S-N nitrogen environments

- **Y6:** Referenced with a -1.24 eV shift, S2p thiophene C-S peaks appeared at 161.6 eV and 162.9 eV, and N-S-N peaks at 162.2 eV and 163.5 eV (Figure 11a). N1s peaks were positioned for $C \equiv N$ at 396.5 eV, C-N at 397.5 eV, and N-S-N at 398.1 eV, with a $\pi - \pi*$ satellite at 399.8 eV (Figure 11b).
- **Y12:** Adjusted with a -1.40 eV shift, S2p thiophene C-S peaks occurred at 161.4 eV and 162.6 eV, and N-S-N peaks at 162.0 eV and 163.1 eV (Figure 12a). N1s $C \equiv N$ peak was located at

Table 4 Theoretical and experimental atomic ratios for the pure donor and acceptor films.

Material	Element	Theoretical (%)	Experimental (%)
Y6	S 2p	29.4	28.6
	N 1s	47.1	45.7
	F 1s	23.5	25.7
Y12	S 2p	29.4	30.2
	N 1s	47.1	44.1
	F 1s	23.5	25.7
PM6	S 2p	80.0	78.1
	F 1s	20.0	21.9
D18-Cl	S 2p	81.8	80.0
	N 1s	18.2	20.0

396.2 eV, C-N at 397.2 eV, and N-S-N at 397.8 eV , with a satellite at 399.4 eV (Figure 12b).



(a) Y6 S2p core-level spectrum.

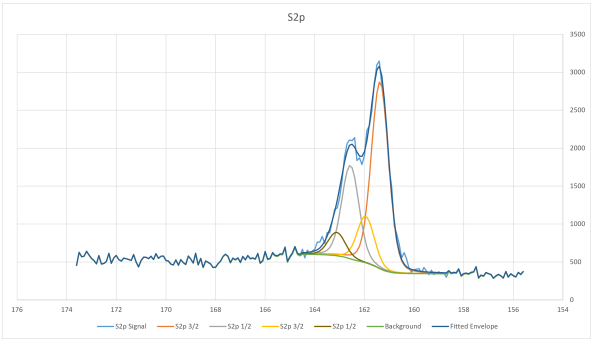
(b) Y6 N1s core-level spectrum.

Figure 11 High-resolution XPS spectra of the pristine Y6 acceptor film.

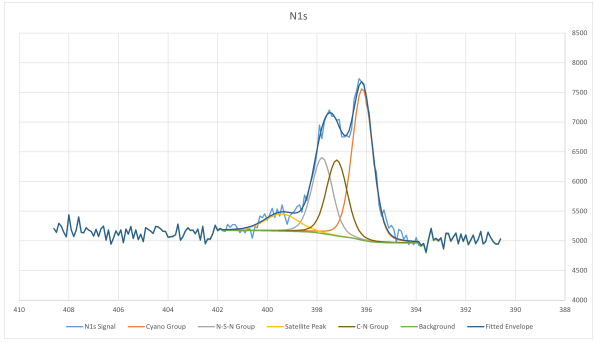
4.3.3 High-resolution Spectra of Donors PM6 and D18-Cl

The core-level spectra for PM6 and D18-Cl, as shown in Figure 13, exhibit $S2p_{3/2} - 2p_{1/2}$ spin-orbit splitting with a 1:2 doublet area ratio and $\Delta = 1.16$ eV.

- **PM6:** Referenced with a -0.86 eV shift, S2p peaks representing both fluorinated and unfluorinated sulfur appeared at 162.2 eV and 163.4 eV (Figure 13a).
- **D18-Cl:** Calibrated with a -1.13 eV shift, S2p thiophene and chlorinated C-S peaks occurred at 161.8 eV and 162.9 eV, and benzothiadiazole N-S-N peaks at 163.2 eV and 164.2 eV, maintaining a 1:8 ratio (Figure 13b).

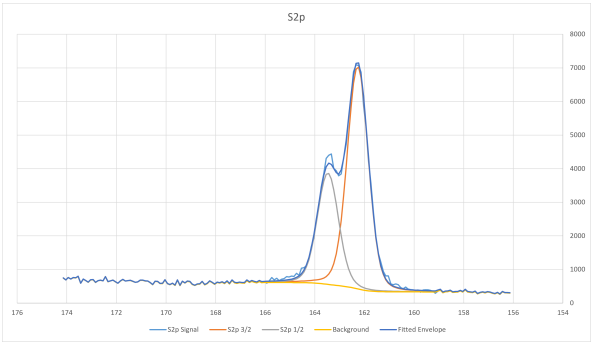


(a) Y12 S2p core-level spectrum.

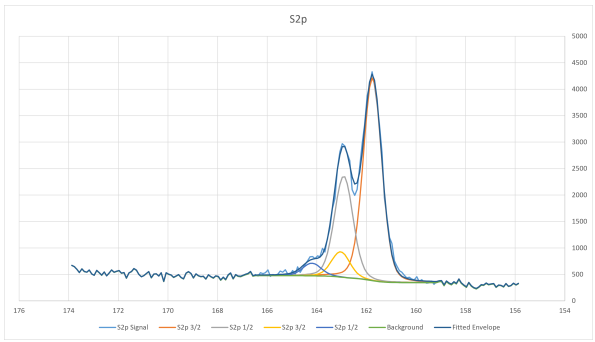


(b) Y12 N1s core-level spectrum.

Figure 12 High-resolution XPS spectra of the pristine Y12 acceptor film.



(a) PM6 S2p core-level spectrum.

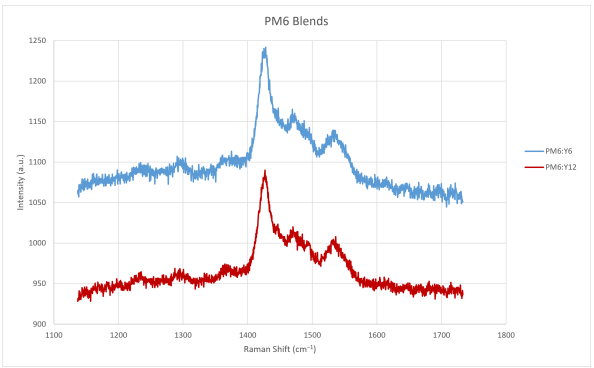


(b) D18-Cl S2p core-level spectrum.

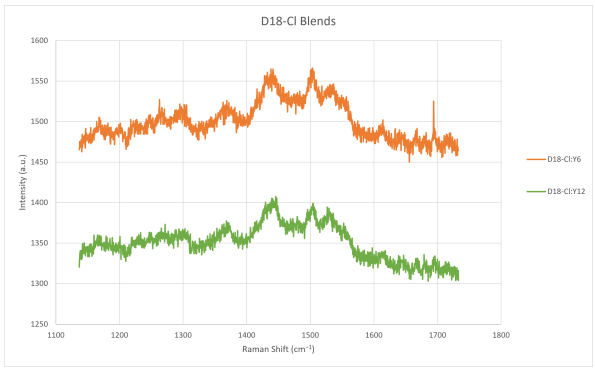
Figure 13 High-resolution XPS spectra of the pristine PM6 and D18-Cl donors films.

4.4 Structural Profiling

Figure 14 presents the Raman spectra for the four BHJ blends: PM6:Y6, PM6:Y12, D18-Cl:Y6, and D18-Cl:Y12. The PM6:Y6 and PM6:Y12 spectra (Figure 14a) are nearly identical, characterized by a sharp, dominant peak at approximately 1428 cm^{-1} and a secondary shoulder near 1470 cm^{-1}. Next, the D18-Cl:Y6 and D18-Cl:Y12 spectra (Figure 14b) demonstrate broader, more complex multiplets. The dominant features for these blends are shifted to higher wavenumbers, with prominent peaks observed around 1438 cm^{-1} and 1504 cm^{-1}.



(a) Raman spectra of PM6 blends.



(b) Raman spectra of D18-Cl blends.

Figure 14 Raman spectra comparison of the PM6 and D18-Cl donor-acceptor blends.

5 Discussion

5.1 Optical Characterization

The normalized absorption profiles confirm that blending broadens the spectral response of active-layer films. Polymer donors harvest visible light via electronic transitions, while non-fullerene acceptors extend absorption into the near-infrared region through intramolecular charge transfer mechanisms. Combining these materials yields thin films capable of complementary photon harvesting, which is essential for maximizing short-circuit current density in organic photovoltaic devices.

5.2 Thermal Stability and Degradation Analysis

The D18-Cl:Y6 blend reaches its maximum absorbance at a lower thermal threshold of 140 °C. At 300 °C, D18-Cl:Y6 undergoes a significant degradation. The PM6:Y6 film demonstrates greater thermal endurance by continuing to densify up to 180 °C. Furthermore, its degradation pathway at extreme temperatures of 300 °C is selectively concentrated within the acceptor component. While the Y6 near-infrared peak is completely destroyed, the PM6 donor framework retains substantial absorption intensity. This selective collapse indicates that Y6 undergoes severe phase separation and chemical decomposition within a relatively resilient PM6 polymer matrix.

Because thermal stressing was conducted on a hot plate for 10 minutes inside a nitrogen glovebox, ambient moisture and oxygen were excluded. This confirms that the severe optical collapse observed at 300 °C stems directly from thermally driven phase separation and intrinsic thermal decomposition of the active layer materials, rather than oxidative degradation.

Overall, both blend systems maintain structural stability up to 180 °C, beyond which progressive thermal degradation impairs optical performance.

5.3 XPS

The XPS analysis successfully validated the chemical integrity of the synthesized pure films. The striking alignment between the experimental atomic percentages and the theoretical stoichiometric ratios confirms that the active layers were highly pure and free from significant degradation.

The core-level deconvolution revealed distinct electronic environments consistent with the molecular architectures of the materials. Furthermore, the prominent $\pi - \pi*$ satellite peaks in the N1s spectra of the acceptors indicate strong intermolecular $\pi - \pi$ stacking within the pristine films, a crucial factor for efficient charge transport.

By defining the exact peak positions, constrained widths, and relative area ratios for these pristine materials, this initial analysis establishes the rigid mathematical constraints necessary to accurately deconvolute and evaluate the complex, overlapping spectra of the fully formulated donor-acceptor blends in subsequent phases of the study.

5.4 Raman Spectroscopy

The recorded Raman spectra primarily reflect the C=C symmetric stretching modes of the conjugated polymer backbones, as their large scattering cross-section dominates the overall signal. The sharp, strongly localized peaks observed in the PM6 blends suggest a high degree of structural order and conformational rigidity within the PM6 domains. This highly ordered

packing indicates strong intermolecular $\pi - \pi$ interactions, which are essential for forming a well-defined blend morphology.

In contrast, the broader, multiplet peak structure present in the D18-Cl blends reflects the more complex fused-ring architecture of the D18-Cl backbone. This indicates a wider distribution of vibrational microstates and a more intermixed amorphous phase, which serves to maximize the donor-acceptor interfacial area. Crucially, substituting the Y6 acceptor with Y12 produces no significant shift in the primary vibrational modes for either donor. This demonstrates that the extended alkyl chains of Y12 do not strongly perturb the in-plane backbone vibrations or the localized phase-packing of the donor polymers.

6 Limitations and Future Work

While this study provides insights into the solution processing, optical properties and thin-film behavior of organic semiconductor blends, several experimental and scope-related limitations were encountered during fabrication and characterization.

A primary technical limitation was caused by electrostatic forces inside the dry nitrogen glove box environment. Although an anti-static gun was used, the residual static electricity continued to interfere with the analytical balance during the mass measurements of the powders. To eliminate this issue in future work, incorporating a permanently mounted active ionizer bar directly over the weighing station will ensure consistency across solution batches.

Additionally, non-homogeneity was observed across the spin-coated thin films, creating noticeable discrepancies in thickness and optical absorption profiles among duplicate samples. This variation was largely attributed to static dispensing and manual solution spreading on the substrates prior to spin coating. To overcome this sample-to-sample variability, subsequent studies should systematically refine the solution dispensing protocol and optimize spin-coating acceleration rates.

Furthermore, the scope of the thermal stability analysis was constrained by time, as thermal degradation experiments were exclusively performed on PM6:Y6 and D18-Cl:Y6 films, leaving the Y-based blends (PM6:Y12 and D18-Cl:Y12) unexamined under thermal stress.

Lastly, while the surface chemistry was comprehensively characterized, standard XPS is highly surface-sensitive and primarily probes the top few nanometers of the active layer. This limits the understanding of vertical phase separation within the bulk heterojunction (BHJ) blends. Future studies should incorporate XPS depth profiling, such as ion sputtering techniques, to elucidate the vertical composition gradients and provide a complete three-dimensional profile of the donor-acceptor distribution throughout the entire film thickness.

Looking towards a broader extension of this project, a promising next step is to integrate these active layers into complete organic photovoltaic device architecture to directly correlate the findings with power conversion efficiency.

7 Acknowledgment

The authors sincerely thank Prof. Dr. Frédéric Laquai, Prof. Dr. Emiliano Cortés, Dr. Shahidul Alam, Dr. Maria Ferree, Edoardo Mariani, and Diya Xie for their guidance and support. This project was conducted at Ludwig Maximilian University of Munich and further supported by KAUST Academy and KA CARE.

8 Conclusion

This research thoroughly examined the optical, structural, and thermal stability of active layers in OSCs, specifically polymer donors PM6 and D18-Cl, and non-fullerene acceptors Y6 and Y12. Testing showed that these paired materials efficiently capture a broad spectrum of light and remain structurally sound until temperatures exceed 180°C. Beyond this threshold, extreme heating causes the materials to heavily separate and break down, with the Y6 components showing particular vulnerability at 300°C. Advanced molecular scanning verified the chemical flawlessness of the unmixed layers and highlighted differing internal architectures: PM6 created stiff, highly organized structures, while D18-Cl promoted a more chaotic, intertwined layout. Importantly, swapping the standard receiver molecule for an alternative version (Y12) did not disturb the foundational structure or the internal arrangement of the original polymers. Ultimately, precision modifications to molecular side-chains can successfully prevent heat-driven physical breakdown, presenting a practical method for boosting the lifespan and market viability of carbon-based solar technologies.

References

[1] Jenny Nelson. *The Physics of Solar Cells*. Imperial College Press, 2003. DOI: 10.1142/p276.

[2] Ossila Ltd. *Organic Photovoltaics Introduction*. https://www.ossila.com/pages/organic-photovoltaics-introduction. 2026.

[3] Fred A. Stevie and Carrie L. Donley. "Introduction to x-ray photoelectron spectroscopy". In: *Journal of Vacuum Science & Technology A* 38.6 (2020), p. 063204.

[4] Qilun Zhang et al. "In situ near-ambient pressure X-ray photoelectron spectroscopy reveals the effects of water, oxygen and light on the stability of PM6:Y6 photoactive layers". In: *Journal of Materials Chemistry C* 11 (2023), pp. 3112–3118.